

Radiation Hydrodynamical Instabilities in Cosmological and Galactic Ionization Fronts

Daniel J. Whalen¹ • Michael L. Norman²

Abstract Ionization fronts, the sharp radiation fronts behind which H/He ionizing photons from massive stars and galaxies propagate through space, were ubiquitous in the universe from its earliest times. The cosmic dark ages ended with the formation of the first primeval stars and galaxies a few hundred Myr after the Big Bang. Numerical simulations suggest that stars in this era were very massive, 25 - 500 solar masses, with H II regions of up to 30,000 light-years in diameter. We present three-dimensional radiation hydrodynamical calculations that reveal that the I-fronts of the first stars and galaxies were prone to violent instabilities, enhancing the escape of UV photons into the early intergalactic medium (IGM) and forming clumpy media in which supernovae later exploded. The enrichment of such clumps with metals by the first supernovae may have led to the prompt formation of a second generation of low-mass stars, profoundly transforming the nature of the first protogalaxies. Cosmological radiation hydrodynamics is unique because ionizing photons coupled strongly to both gas flows and primordial chemistry at early epochs, introducing a hierarchy of disparate characteristic timescales whose relative magnitudes can vary greatly throughout a given calculation. We describe the adaptive multistep integration scheme we have developed for the self-consistent transport of both cosmological and galactic ionization fronts.

Daniel J. Whalen

Michael L. Norman

¹Department of Physics, Carnegie Mellon University, Pittsburgh, PA 15213

²Center for Astrophysics and Space Sciences, University of California at San Diego, La Jolla, CA 92093

1 First Light and the Rise of Primeval Galaxies

State of the art numerical simulations reveal that the first stars in the universe formed in isolation in small cosmological halos (spheroidal bound clumps of dark matter and H/He gas) at redshifts $z \sim 20 - 30$, or 200 - 400 Myr after the Big Bang (Abel et al. 2002; Bromm et al. 2002; Nakamura & Umemura 2001). Soon thereafter, gravitational mergers congregated these star forming halos into the first primitive galaxies. Preliminary results from minihalo collapse models suggest that primordial (or Pop III) stars were very massive, 25 - 500 M_{\odot} (O'Shea & Norman 2007). They created H II regions that were enormous in comparison to those in the Galaxy today, 2.5 - 5 kpc in radius (Whalen, Abel, & Norman 2004; Kitayama et al. 2004; Alvarez et al. 2006; Abel et al. 2007). Primeval ionization fronts, or I-fronts, were key to the rise of the first protogalaxies for several reasons. First, Pop III stars lacked strong winds, so their H II regions determined their circumstellar environments. They regulated the flow of the first heavy elements from primordial supernovae (SNe) into the early IGM (Greif et al. 2007, 2010) and may even have resulted in the prompt formation of a second generation of low-mass stars in SNe remnants (Whalen et al. 2008b). Second, the minihalos forming the first stars themselves coalesced in small swarms due to cluster bias. Radiation fronts from one star in the cluster could engulf nearby halos, photoevaporating them to varying degrees and either suppressing or allowing new star formation in them (Shapiro et al. 2004; Iliiev et al. 2005; Susa & Umemura 2006; Whalen et al. 2008a; Susa et al. 2009; Whalen et al. 2010). Thus, cosmological I-fronts in part governed the number and character of stars that were swept up into the first primitive galaxies.

Once primeval galaxies formed and sustained cyclical star formation, they too propagated I-fronts into

the IGM, beginning the process of cosmological reionization by which the cold, neutral, mostly featureless universe of the recombination era was gradually transformed into the hot, transparent cosmic web of galaxies and clusters of galaxies we observe today (Ricotti et al. 2002, 2008; Wise & Abel 2008; Wise & Cen 2009). Recent numerical models have demonstrated that the I-fronts of both individual Pop III stars and protogalaxies formed H_2 in their outer layers, a key coolant at high redshifts that may have seeded the formation of additional structure in the early universe (Ricotti et al. 2001; Whalen & Norman 2008b). High-redshift I-fronts thus influenced the rise of structure on a variety of spatial scales in the early cosmos.

In the Galaxy today, I-fronts from massive stars in the molecular cores of giant molecular clouds (GMCs) are thought to trigger new star formation by perturbing nearby cores on the verge of gravitational collapse (Dale et al. 2007; Gritschneider et al. 2009). In this manner, successive fronts can set off a chain of star formation throughout the cloud. On the other hand, dynamical instabilities in the fronts may degenerate into turbulent flows that support gas against collapse, offsetting triggered star formation. Yet, these same instabilities can form clumps that may later collapse into stars. How ionized flows regulate star formation in the Milky Way today remains to be fully understood.

2 Ionizing Radiation Hydrodynamics in ZEUS-MP

We perform our ionization front calculations with ZEUS-MP (Whalen & Norman 2006), a massively parallel Eulerian astrophysical hydrodynamics code that solves the equations of ideal fluid dynamics¹:

$$\frac{\partial \rho}{\partial t} = -\nabla \cdot (\rho \mathbf{v}) \quad (1)$$

$$\frac{\partial \rho v_i}{\partial t} = -\nabla \cdot (\rho v_i \mathbf{v}) - \nabla p - \rho \nabla \Phi - \nabla \cdot \mathbf{Q} \quad (2)$$

$$\frac{\partial e}{\partial t} = -\nabla \cdot (e \mathbf{v}) - p \nabla \cdot \mathbf{v} - \mathbf{Q} : \nabla \mathbf{v}. \quad (3)$$

Here, ρ , e , and the v_i are the mass density, internal energy density, and velocity at each mesh point and $p = (\gamma - 1)e$ and \mathbf{Q} are the gas pressure and the von Neumann-Richtmeyer artificial viscosity tensor. ZEUS-MP evolves these equations with a second-order accurate monotonic advection

scheme in one, two, or three dimensions on Cartesian (XYZ), cylindrical (ZRP), or spherical polar (RTP) coordinate meshes. Our augmented version of the publicly-available code self-consistently couples primordial gas chemistry (Whalen & Norman 2008a) and multifrequency photon-conserving UV radiative transfer (Whalen & Norman 2008b) to fluid dynamics for the radiation hydrodynamical transport of cosmological I-fronts.

2.1 Primordial H and He Chemistry

We evolve H, H^+ , He, He^+ , He^{2+} , H^- , H_2^+ , H_2 , and e^- with nine additional continuity equations and the nonequilibrium rate equations of Anninos et al. (1997):

$$\frac{\partial \rho_i}{\partial t} = -\nabla \cdot (\rho_i \mathbf{v}) + \sum_j \sum_k \beta_{jk}(T) \rho_j \rho_k - \sum_j \kappa_j \rho_j, \quad (4)$$

where β_{jk} is the rate coefficient of the reaction between species j and k that creates (+) or destroys (-) species i , and the κ_j are the radiative rate coefficients. We assume that the species share a common velocity distribution. Mass and charge conservation, which are not guaranteed by either chemical or advective updates, are enforced each time the fluid equations are solved.

Microphysical heating and cooling due to photoionization and gas chemistry is coupled to the gas energy density by an isochoric update that is operator-split from updates to the fluid equations:

$$\dot{e}_{\text{gas}} = \Gamma - \Lambda, \quad (5)$$

where Γ is the cumulative heating rate due to photons of all frequencies and Λ is the sum of the cooling rates due to collisional ionization and excitation of H and He, recombinations of H and He, inverse Compton scattering (IC) from the CMB, bremsstrahlung emission, and H_2 cooling.

2.2 Radiative Transfer

Our photon-conserving UV transport (Mellema et al. 2006; Abel, Norman, & Madau 1999), which is distinct from the flux-limited diffusion native to the public release of ZEUS-MP, solves the static approximation to the equation of transfer in flux form to compute radiative rate coefficients for the reaction network at every point on the coordinate mesh. As currently implemented, our code can transport photons from a point source centered in a spherical grid or in plane waves along the x or z -axes of Cartesian or cylindrical meshes. To model Pop III spectra, we discretize

¹<http://lca.ucsd.edu/portal/codes/zeusmp2>

the blackbody photon emission rates of a star with 40 uniform bins from 0.755 to 13.6 eV and 80 logarithmically spaced bins from 13.6 eV to 90 eV, normalizing them by the total ionizing photon rates by Schaerer (2002). The radiative reactions in our models are listed in Table 1 of Whalen & Norman (2008b). We calculate H_2 photodissociation rates along rays parallel to the direction of radiation flow using self-shielding functions modified for thermal broadening as prescribed by Draine & Bertoldi (1996) to approximate the effects of gas motion. They are shown in equations 9 and 10 of Whalen & Norman (2008b).

2.3 Radiation Forces

Radiation pressure due to ionizations occurs at the I-front itself and in recombining gas in the H II region. Whalen & Norman (2006) found that the acceleration of fluid elements at the front was large but momentary, and only alters the velocity of the front by 1 - 2 km s⁻¹. Momentum deposition within the H II region is only prominent where gas is very dense, like at the center of a minihalo being evaporated by its star. There, rapid successive cycles of ionization and recombination can impart radiation forces to the gas that are hundreds of times the strength of gravity at early times (lower left panel of Figure 1 in Kitayama et al. 2004). As these forces propel gas near the center of the halo out into the H II region, its densities and recombination rates fall, so more ionizing photons from the star reach the I-front. This higher flux results in I-fronts that are faster than when such forces are not included. In UV breakout from the first star-forming halos, radiation forces speed up the D-type I-front by 10 - 20%. However, this effect is transient: after the internal rearrangement of gas deep within the H II region dilutes its interior, radiation forces there sharply fall (see also Krumholz & Matzner 2009; Draine 2010; Lopez et al. 2010). We describe the timescales on which momentum updates are performed below.

2.4 Adaptive Subcycling

A hierarchy of highly disparate characteristic time scales arises when gas dynamics, radiative transfer, and primordial chemistry are solved in a given application. The three governing times are the Courant time, the chemical time

$$t_{chem} = 0.1 \frac{n_e + 0.001n_H}{\dot{n}_e}, \quad (6)$$

and the photoheating/cooling time

$$t_{hc} = 0.1 \frac{e_{gas}}{\dot{e}_{ht/cool}}. \quad (7)$$

Their relative magnitudes can seamlessly evolve during a single application. For example, when an I-front propagates through a medium, photoheating times are often smaller than Courant times, and chemical time scales are usually shorter than either one. On the other hand, fossil H II regions can cool faster than they recombine, so cooling times become shorter than chemical times. The key to solving all three processes self-consistently is to evolve each on its own timescale without restricting the entire algorithm to the shortest of the times. To successfully deal with both I-fronts and relic H II regions, an algorithm must adaptively reshuffle the time scales on which the three processes are solved. Implicit schemes are sometimes applied to stiff sets of differential equations like those in our model because they are unconditionally stable over the Courant time. However, accurate I-front transport in stratified media often requires restricting updates to both the gas energy and fluid equations to photoheating times in order to capture the correct energy deposition into the gas, and linear system solves over such short time scales would be prohibitive in more than one or two dimensions. Enforcing photon conservation in implicit schemes can also be problematic.

We instead subcycle chemical species and gas energy updates over the minimum of the chemical and heating/cooling times until the larger of the two has been crossed, at which point we perform full hydrodynamical updates of gas densities, energies, and velocities. These times are global minima for the entire grid. The chemical times are defined in terms of electron flow to accommodate all chemical processes rather than just ionizations or recombinations. Adopting the minimum of the two times for chemistry and gas energy updates enforces accuracy in the reaction network when t_{chem} becomes greater than t_{hc} , such as in relic H II regions. Our adaptive subcycling scheme is described in greater detail in (Whalen & Norman 2008a).

3 Ionization Front Instabilities

When a point source of monoenergetic ionizing photons appears in a uniform H and He medium, they are not free to simply stream into the interstellar medium (ISM) because of the large cross section to photoionization in the gas. Instead, they emerge as a sharp wall of radiation, behind which gas is almost fully ionized and heated to a few $\times 10^4$ K and beyond which it is completely neutral. The thickness of the I-front separating the neutral and ionized gas is a few mean free paths of the ionizing photons through the neutral gas. The initial propagation of the I-front through the gas

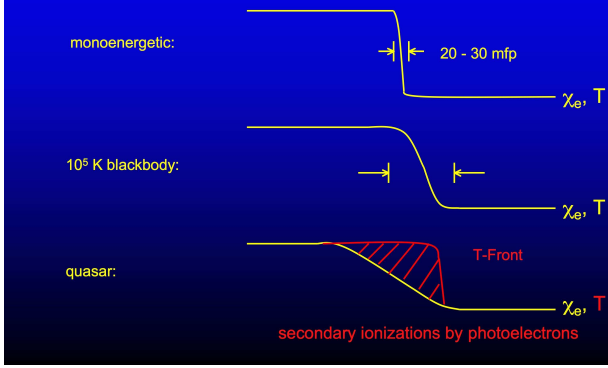


Fig. 1 The structure of an ionization front. χ_e denotes ionized fraction and T is gas temperature. Top: monoenergetic UV photons just above the ionization edge of H. Center: a 10^5 K Pop III star blackbody spectrum. Note the significant broadening of the front. Bottom: power-law quasar x-ray source spectrum. Note that in the first two cases that temperature tracks the ionization fraction, but not in the quasar case. Here, hard photons penetrate well ahead of the front, strongly heating but not significantly ionizing the gas.

is supersonic in that the ionization wave advances far more quickly than any hydrodynamic response by the hot gas in its wake. This is known as an R-type I-front. As the front recedes from the star it slows, partly due to geometric dilution of the ionizing flux and partly because recombinations in the ionized gas remove photons that would otherwise have gone on to advance the front. If the medium is static (no gas motion allowed), the I-front comes to a halt when the H II region it bounds encloses enough ionized gas that the global recombination rate equals the emission rate of source photons. The radius at which this occurs is known as the Strömgren radius.

In reality, as the I-front slows to the Strömgren radius the pressure wave that has built up in the hot ionized gas behind it overtakes it and passes through it, steepening into a shock as it does so. Thereafter, the H II region expands subsonically with respect to the sound speed in its interior, which is still supersonic with respect to the ambient neutral gas. As it expands, it bypasses the static Strömgren radius limit because its interior densities and therefore recombination rates fall, allowing source photons to continue to stream to the front. As the H II region grows it pushes aside more and more ambient gas which accumulates on its surface, causing the shock to detach from and move ahead of the I-front. This is known as a D-type I-front.

3.1 Thin-Shell Instabilities

If this shocked neutral shell can radiatively cool, it will collapse into a cold dense layer that is prone to

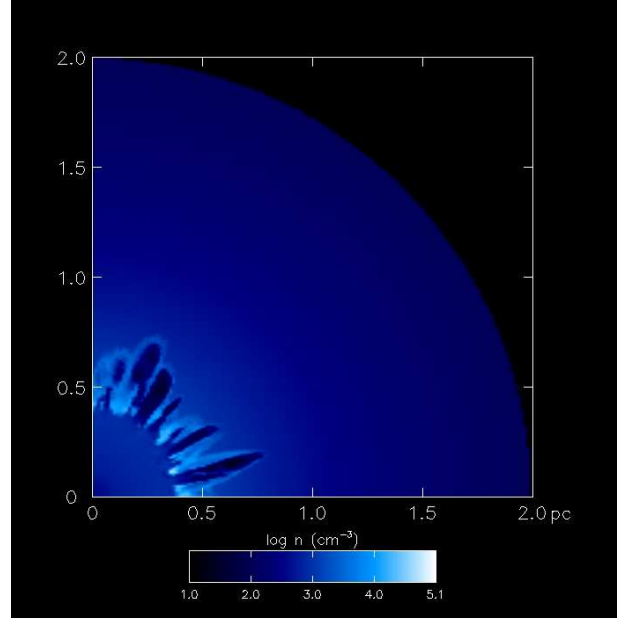
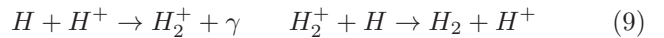
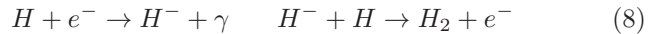


Fig. 2 Thin-shell instability in a primordial I-front mediated by H_2 cooling.

fragmentation via Vishniac, or thin-shell, instabilities (Vishniac 1983). Unlike similar features in the dense shells of astrophysical blast waves, these erupt into very violent instabilities because ionizing radiation opportunistically escapes through the cracks in the shell in jets ahead of the front (Garcia-Segura & Franco 1996; Whalen & Norman 2008a). These jets rapidly crumple into complicated flows that form dense clumps that can persist for the life of the star. In the Galaxy today, metals and dust radiatively cool the shell and trigger such instabilities. Cooling by atomic H and He lines in the shocked gas of cosmological I-fronts by itself is too weak to incite such instabilities. However, they can instead form by H_2 cooling.

Primordial I-fronts are driven by hard UV sources whose photons have a variety of mean free paths through neutral gas. Collectively, they broaden the front, which leads to ionized fractions of 10% and temperatures of 2000 - 3000 K in its outer layers as we illustrate in Figure 1. These are ideal conditions for gas phase catalysis of H_2 by the H^- and H_2^+ channels:



Although much less efficient than metals, H_2 is a far more effective coolant than H and He lines at 3000 K; sandwiched between the front and the shocked neutral shell, it cools the base of the shell sufficiently to

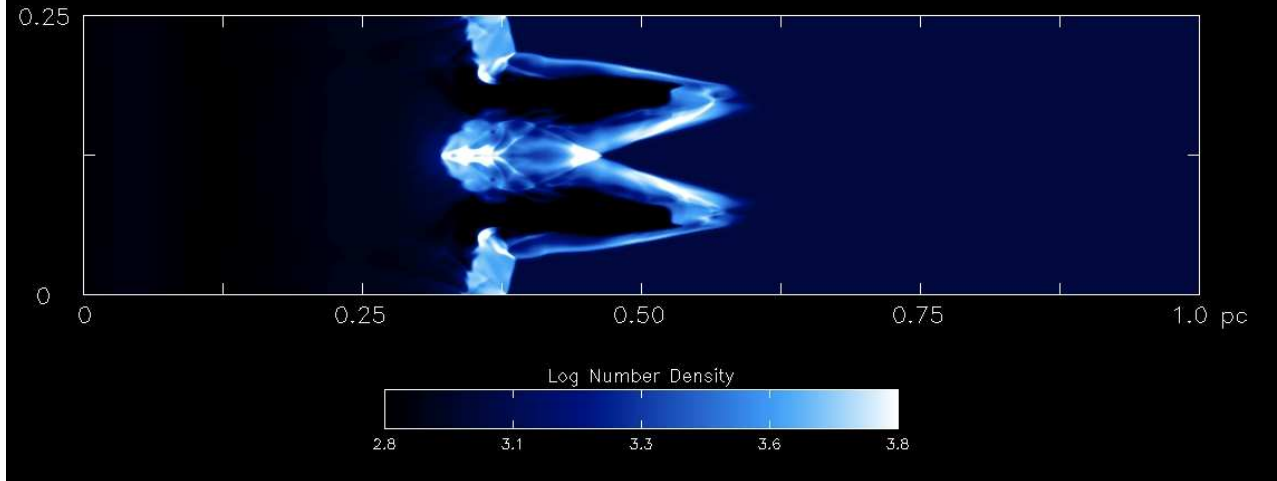


Fig. 3 The shadow instability.

trigger thin-shell overstabilities that erupt into violent radiation-driven instabilities, as we show in Figure 2 (Whalen & Norman 2008b). In this simulation, we center a 10^5 K blackbody UV source approximating a $120 M_{\odot}$ Pop III star in a H/He gas profile similar to that of a cosmological minihalo. When the front becomes D-type, instabilities due to H_2 cooling can be seen to appear at the base of the dense shell. More models are required to determine if the turbulent gas clumps survive until the death of the star and are prone to gravitational collapse.

3.2 Shadow Instabilities

In Figure 3 we show the breakout of a second kind of radiation hydrodynamical instability in primordial I-fronts, the shadow instability (Williams 1999; Whalen & Norman 2008b). These form when density perturbations are advected through an R-type front. The perturbation does not trap the front, it merely dimples it. The walls of the dimple are exposed to a smaller ionizing flux because they are oblique to it; as a consequence, the walls of the dimple transition to D-type before the tip does, causing the tip to advance and elongate the dimple into a jet that abruptly breaks down into a violent instability. Such phenomena would have been unavoidable in the primeval universe, on scales ranging from UV breakout from the first star-forming halos to 100 kpc protogalactic I-fronts. The role of H_2 formation, thin-shell instabilities, and shadow instabilities in structure formation in early cosmological flows remains to be properly investigated.

3.3 AOI Instabilities

We show in Figure 4 the radiation front of a $25 M_{\odot}$ Pop III star enveloping a nearby star-forming halo

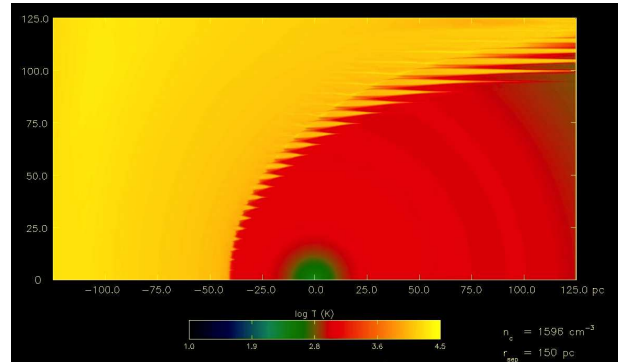


Fig. 4 Angle of incidence (AOI) instabilities in the ionization front of a Pop III star enveloping a neighbor halo.

(Whalen et al. 2010). Spikes in the front can be seen all along the arc surrounding the halo, but are increasingly prominent with altitude above its axis. This is an example of an I-front instability described by Williams (2002), in which photons that arrive at the front at any angle other than 90° cause it to be unconditionally unstable: an angle of incidence (AOI) instability. Detailed linear perturbation analysis predicts that the greater the angle of deviation of the photons from pure incidence, the faster the growth of the unstable mode, which is true of the protrusions in Figure 4. In this example, the unstable modes have little effect on star formation in the halo because those closest to its core have the smallest amplitudes and fail to puncture it. Dynamical instabilities have also been found in I-fronts engulfing Galactic molecular cloud cores in numerical models, but gas in those simulations could efficiently cool by fine-structure lines (Mizuta et al. 2005, 2006) so the unstable modes are likely thin-shell in origin.

References

- Abel, T., Norman, M. L., & Madau, P. 1999, *Astrophys. J.*, 523, 66
- Abel, T., Bryan, G. L., & Norman, M. L. 2002, *Science*, 295, 93
- Abel, T., Wise, J. H., & Bryan, G. L. 2007, *Astrophys. J. Lett.*, 659, L87
- Alvarez, M. A., Bromm, V., & Shapiro, P. R. 2006, *Astrophys. J.*, 639, 621
- Anninos, P., Zhang, Y., Abel, T., & Norman, M. L. 1997, *New Astronomy*, 2, 209
- Bromm, V., Coppi, P. S., & Larson, R. B. 2002, *Astrophys. J.*, 564, 23
- Dale, J. E., Bonnell, I. A., & Whitworth, A. P. 2007, *Mon. Not. R. Astron. Soc.*, 375, 1291
- Draine, B. T. 2010, arXiv:1003.0474
- Draine, B. T., & Bertoldi, F. 1996, *Astrophys. J.*, 468, 269
- Garcia-Segura, G., & Franco, J. 1996, *Astrophys. J.*, 469, 171
- Greif, T. H., Johnson, J. L., Bromm, V., & Klessen, R. S. 2007, *Astrophys. J.*, 670, 1
- Greif, T. H., Glover, S. C. O., Bromm, V., & Klessen, R. S. 2010, *Astrophys. J.*, 716, 510
- Gritschneider, M., Naab, T., Walch, S., Burkert, A., & Heitsch, F. 2009, *Astrophys. J. Lett.*, 694, L26
- Iliev, I. T., Shapiro, P. R., & Raga, A. C. 2005, *Mon. Not. R. Astron. Soc.*, 361, 405
- Kitayama, T., Yoshida, N., Susa, H., & Umemura, M. 2004, *Astrophys. J.*, 613, 631
- Krumholz, M. R., & Matzner, C. D. 2009, *Astrophys. J.*, 703, 1352
- Lopez, L. A., Krumholz, M., Bolatto, A., Prochaska, J. X., & Ramirez-Ruiz, E. 2010, *Bulletin of the American Astronomical Society*, 42, 261
- Mellema, G., Iliev, I. T., Alvarez, M. A., & Shapiro, P. R. 2006, *New Astronomy*, 11, 374
- Mizuta, A., Kane, J. O., Pound, M. W., Remington, B. A., Ryutov, D. D., & Takabe, H. 2005, *Astrophys. J.*, 621, 803
- Mizuta, A., Kane, J. O., Pound, M. W., Remington, B. A., Ryutov, D. D., & Takabe, H. 2006, *Astrophys. J.*, 647, 1151
- Nakamura, F., & Umemura, M. 2001, *Astrophys. J.*, 548, 19
- O'Shea, B. W., & Norman, M. L. 2007, *Astrophys. J.*, 654, 66
- Ricotti, M., Gnedin, N. Y., & Shull, J. M. 2001, *Astrophys. J.*, 560, 580
- Ricotti, M., Gnedin, N. Y., & Shull, J. M. 2002, *Astrophys. J.*, 575, 33
- Ricotti, M., Gnedin, N. Y., & Shull, J. M. 2008, *Astrophys. J.*, 685, 21
- Schaerer, D. 2002, *Astron. Astrophys.*, 382, 28
- Shapiro, P. R., Iliev, I. T., & Raga, A. C. 2004, *Mon. Not. R. Astron. Soc.*, 348, 753
- Susa, H., & Umemura, M. 2006, *Astrophys. J. Lett.*, 645, L93
- Susa, H., Umemura, M., & Hasegawa, K. 2009, *Astrophys. J.*, 702, 480
- Vishniac, E. T. 1983, *Astrophys. J.*, 274, 152
- Whalen, D., Abel, T., & Norman, M. L. 2004, *Astrophys. J.*, 610, 14
- Whalen, D., & Norman, M. L. 2006, *Astrophys. J. Suppl. Ser.*, 162, 281
- Whalen, D., O'Shea, B. W., Smidt, J., & Norman, M. L. 2008, *Astrophys. J.*, 679, 925
- Whalen, D., van Veelen, B., O'Shea, B. W., & Norman, M. L. 2008, *Astrophys. J.*, 682, 49
- Whalen, D. J., & Norman, M. L. 2008, *Astrophys. J.*, 672, 287
- Whalen, D., & Norman, M. L. 2008, *Astrophys. J.*, 673, 664
- Whalen, D., Hueckstaedt, R. M., & McConkie, T. O. 2010, *Astrophys. J.*, 712, 101
- Williams, R. J. R. 1999, *Mon. Not. R. Astron. Soc.*, 310, 789
- Williams, R. J. R. 2002, *Mon. Not. R. Astron. Soc.*, 331, 693
- Wise, J. H., & Abel, T. 2008, *Astrophys. J.*, 684, 1
- Wise, J. H., & Cen, R. 2009, *Astrophys. J.*, 693, 984